Oxidation of Ni-Cr alloy at intermediate oxygen pressures. II. Towards the lifetime prediction of alloys

Eric Schmucker, Carine Petitjean, Laure Martinelli, Pierre-Jean Panteix, Sabah Ben Lagha, Michel Vilasi

Oxidation of Ni-Cr alloy at intermediate oxygen pressures. II. Towards lifetime prediction of alloys.

Eric Schmucker[a,c*], Carine Petitjean[a], Laure Martinelli[b], Pierre-Jean Panteix[a], Sabah Ben Lagha[c], Michel Vilasi[a]

[a] *IJL-UMR 7198, Département CP2S, Equipe 206 (Surface et Interface: Réactivité Chimique des Matériaux), B.P. 70239 – F-54506 Vandœuvre les Nancy Cedex, FRANCE.*

[b] *CEA, Université Paris-Saclay, Den-Service de la Corrosion et du Comportement des Matériaux dans leur Environnement (SCCME), F-91191, Gif-sur-Yvette, FRANCE.*

[c] *AREVA NC, Tour Areva, 1 Place Jean Millier, F-92084, Paris-La-Défense Cedex, FRANCE*

*corresponding author
e-mail: eric.schmucker@univ-lorraine.fr; phone: + 33 (0) 3 83 68 46 69; fax: + 33 (0) 3 83 68 46 11

Abstract

The formation of protective Cr_2O_3 layer on Ni-Cr alloys depends on (i) the chromium concentration at the alloy/oxide interface and (ii) the chromium diffusion in the alloy from the core towards the surface. A sufficient interfacial chromium content and chromium gradient are necessary to sustain the selective external oxidation of chromium. Ni-30Cr samples have been oxidised at 1150 °C in 10^{-13} up to 10^{-3} atm O_2. Analytical methods are used to model the diffusion in steady-state conditions and to predict the lifetime of the alloy. The interdiffusion coefficient is found equal to 1.2 x 10^{-10} cm^2 s^{-1}.

Keywords: A. alloy; B. EPMA; B. modelling studies; C. high temperature corrosion; C. selective oxidation.

List of symbols

x	position in the alloy with respect to the alloy/oxide interface (cm)
t	oxidation time (s)
X_{pores}	pores formation depth (µm)
X_{Cr}	chromium depletion depth (µm)
W_{Cr}^{i}	weight chromium content in the alloy at the alloy/oxide interface (wt.%)

N_{Cr}^{i}	atomic chromium fraction in the alloy at the alloy/oxide interface (-)
N_{Cr}°	atomic chromium fraction in the as-prepared alloy (-)
$N_{Cr(x,t)}$	atomic chromium fraction in the alloy at the position x after time t (-)
J_V	vacancy flux
J_{Cr} / J_{Ni}	chromium / nickel flux
k_{pe}	parabolic rate constant for oxidation ($cm^2\ s^{-1}$)
k_c	parabolic rate constant for the alloy/oxide interface recession ($cm^2\ s^{-1}$)
$\tilde{D}$	Interdiffusion coefficient ($cm^2\ s^{-1}$)
V	Molar volume ($cm^3\ mol^{-1}$)
R	Ideal gas constant ($J\ mol^{-1}\ K^{-1}$)
T	Temperature (K)
g^*	critical oxide fraction in the alloy for internal/external oxidation transition (-)
v	stoichiometric coefficient of MO_v oxide (-)
$N_O^{(s)}$	atomic oxygen fraction in the alloy (-)
D_O	oxygen diffusion coefficient in the alloy ($cm^2\ s^{-1}$)

Introduction

One of the major high temperature industrial concerns for materials engineering is to predict the lifetime of the process components. These latter are generally submitted to harsh thermal and mechanical stresses during service, in addition to environmentally induced corrosion. Corrosion phenomenon can cause the end of life of the alloy by excessive consumption of protective elements (*i.e.* which can form slow-growing oxides when oxidised, for instance Cr, Si and Al). Therefore the alloy is not able to form protective oxide anymore but only rapidly growing oxides (e.g. Ni, Fe oxides…) leading to breakaway oxidation [1,2]. Moreover, mechanical failure of the oxide can occur due to thermal and/or growth stresses [3,4]. Compressive stresses arise during oxide growth since the volume of oxide formed is generally higher than the volume of consumed metal, *i.e.* a Pilling and Bedworth ratio superior to the unity. Thermal stresses are originated from the mismatch of the thermal expansion coefficients between the oxide and the alloy. These stresses can result in oxide spallation and then in accelerated oxidation above desquamated sites. For example, in cyclic oxidation conditions both thermal and growth stresses are encountered [5,6]. Lifetime limitations can also arise from failure of the alloy itself, e.g. creep rupture under mechanical loading [7]. Chromia-forming Ni-based superalloys are generally used since they meet prerequisite for

such extreme applications. Indeed, chromium oxide, Cr_2O_3, is a slow-growing protective oxide that can withstand the degradation by molten salts or glasses as well as the corrosion by aggressive atmospheres (metal dusting, gas burners, etc…). In addition, the mechanical properties of these alloys can be improved, for instance, by addition of carbides [8].

When selective oxidation of chromium occurs in chromia-forming alloys, a chromium depleted zone is created underneath the surface with a concentration gradient. Selective external oxidation of chromium is then maintained as long as the flux of chromium towards the alloy/scale interface is high enough to counterbalance the metal loss supplying the oxide growth. Therefore, the study of chromium depletion profiles in alloys oxidised at high temperature has received a great interest from several authors. Analytical solutions coming from Wagner's equations [9,10] have been used to model depletion profiles [11-13]. More recently, numerical methods have been developed for the same purpose [13-18]. Most of the authors have given solutions for steady-state conditions with a moving alloy/scale interface (in cases where metal consumption or vacancies annihilation lead to an alloy/scale interface recession) [11,13-16]. However, Gesmundo *et al.* have given an analytical solution for the case of transient oxidation with a fixed alloy/scale interface [12]. Moreover, a numerical model has been develop to calculate concentration profiles of both elements and vacancies in the alloy depending on quantity of annihilated vacancies at the alloy/scale interface and in the alloy [19].

This paper is the second part of a global study of the oxidation of a model binary Ni-30Cr alloy. Oxidation tests have been performed in several intermediate oxygen partial pressures ranging from 10^{-13} up to 10^{-3} atm O_2 at 1150 °C. Protective oxidation behaviour is observed with the formation of a Cr_2O_3 layer. The first part of this study dealt with the oxidation kinetics and the diffusional mechanisms in the oxide layer [20]. In this part, the attention is focused on the diffusion phenomena in the alloy. The aim of this paper is to propose a method to estimate the chemical lifetime of alloys submitted to high temperature corrosion. This method is based on the establishment of Wagner's and Bastow's [ref] criterions for the selective and continuous formation of the protective oxide, Cr_2O_3. These criterions are based on calculation of critical chromium contents at the alloy/oxide interface and in the core of the alloy. In order to evaluate these critical concentrations, the chromium depletion profiles in the alloy are analysed and the interdiffusion coefficient is calculated. Eventually, an overview of the oxidation-induced phenomena is made based on the results from this paper and the first part of this work [20].

Materials and methods

The same Ni-30Cr alloy as in part I of this study has been used [20]. An ingot was synthesised from pure chromium (99.99% purity, Alfa Aesar) and pure nickel (99.95% purity, Alfa Aesar) by high frequency induction melting under argon atmosphere. The composition of the alloy was verified by EDX analyses and the chromium content was found to be equal to 30.5 ± 1.2 wt.%. For such a composition and at temperatures superior to 800 K, this alloy is a single phased, austenitic (f.c.c.), solid solution of chromium in nickel [21]. Before oxidation tests, samples were cut from the ingot with dimensions around 8 x 8 x 1.5 mm and ground with P1200 SiC paper. In order to reveal its microstructure, the alloy was chemically etched in *aqua regia* for 60 seconds. It was then washed in deionized water and ethanol before observation. The microstructure of the as-prepared alloy is coarse with a grain size of several hundreds of micrometres (Fig. 1).

Oxidation experiments have been performed in Rhines packs in different oxygen atmospheres: 5.9×10^{-3}; 4.2×10^{-10}; 5.8×10^{-12} and 2.8×10^{-13} atm. More details about the experimental device for oxidation are given in [20]. After the oxidation tests, samples were cut in cross sections and embedded in epoxy resin. Resins were ground by using SiC paper from grit P400 to P1200, then diamond polishing was applied with grit size from 9 µm down to 1 µm. Final mirror polishing was made with colloidal silica.

Microscopic characterisations have been performed with a field-effect SEM, Schottky emission JEOL J7600F. Chemical analyses of the elementary profiles in the alloy have been performed with an acceleration voltage of 20 kV and an EDS detector (Silicon Drift Detector) by SEM or with a WDS detector with an SX100 EPMA. Pure chromium and nickel metals were used as standards.

Results

The oxidation kinetics of Ni-30Cr alloy at 1150 °C in oxygen pressures comprised between 10^{-13} and 10^{-2} atm have been investigated in part I of this study [20]. The parabolic rate constant for oxidation has been found to be independent on the oxygen pressure with an average value of 5.0×10^{-12} cm^2 s^{-1}. In addition, the oxide growth mechanism has been

identified as an outward diffusion of chromium interstitials, mainly along the oxide grain boundaries.

The cross-section backscattered electrons (BSE) image in Fig. 2 shows the typical feature of the oxidised alloy. A protective, homogeneous, compact and adherent chromium oxide layer has grown at the surface of the alloy. Numerous pores are clearly visible in the subsurface of the alloy. These pores were not initially present in the alloy, so they have emerged during the oxidation treatment. It is noteworthy that the depth of the pores formation (X_{pores}) increases with the oxidation duration in all studied atmospheres (Table 1). The pores formation depth is evaluated as the approximate maximum depth where pores are observed (Fig. 2). In addition, pores generally appears at about 10 µm from the alloy/scale interface and the extent of pores presence is comprised between the half and the whole chromium depletion depth (X_{Cr}).

The chromium depletion profiles in the alloy after oxidation have been obtained from EDX and WDX analyses (Fig. 3a to d). In every tested atmosphere, the evolution of the chromium depletion profiles exhibits the same feature. First, the chromium depletion depth logically increases with time, as chromium diffuses from the bulk alloy towards the alloy/scale interface during oxidation. The depletion depth X_{Cr} (Table 1) reaches about 500 µm after 289 h of oxidation. Secondly, the chromium content W_{Cr}^{i} at the alloy/scale interface reaches a quite low value between 12 and 15 wt.% after only 1 h of oxidation. This content then increases until stabilization around 23 wt.% after about 49 h of oxidation. For longer durations, the system is then in steady-state regime. Values for chromium content at the interface (W_{Cr}^{i}), chromium depletion depth (X_{Cr}) and pores formation depth (X_{pores}) are compiled in Table 1. It must be pointed out that the chromium interfacial content values are obtained by fitting profiles with Eq. 6 and not by direct reading on the profiles (see discussion).

A comparison of chromium depletion profiles after 100 h of oxidation in different oxygen partial pressures is given in Fig. 4. From Fig. 3 and 4, it clearly appears that the depletion profiles are very similar whatever the oxygen pressure is.

Discussion

1. Pores formation

The presence of pores in the alloy after oxidation of Ni-Cr alloys has been previously reported by other authors [22,23]. The formation of voids in metal or alloys is known to arise after the accumulation of metal vacancies on sinks such as grain boundaries or dislocation loops [19]. Two possible sources of metal vacancies can be encountered during high temperature oxidation of alloys. First, in the case of oxides growing by cationic diffusion, when a metal atom enters the oxide, a metal vacancy is created at the alloy/scale interface and can thus be injected in the alloy if not directly annihilated at this interface. Second, the selective oxidation of chromium leads to chromium depletion in the alloy, leading to a chromium flux (J_{Cr}) from the core of the alloy towards the alloy/scale interface. In addition, a symmetric nickel profile is consequently obtained and the resulting flux of nickel (J_{Cr}) is oriented towards the core of the alloy. If a mismatch between the intrinsic diffusion coefficients of the constituents of the alloy exists, an unbalance is created between the matter fluxes. In order to balance these fluxes, a vacancies flux (J_V) is then created and oriented in the opposite direction of the fastest diffusing element. This phenomenon is known as the Kirkendall effect [24]. In f.c.c. Ni-Cr alloys, chromium diffuses faster than nickel [25,26], vacancies are thus diffusing towards the core of the alloy, with $J_V = -J_{Cr} - J_{Ni}$ (Fig.5). This is consistent with the increase of the observed pores formation depth with time (Table 1).

2. Interdiffusion coefficient

Since the protection against oxidation is ensured as long as enough chromium is brought from the alloy to its surface for selective external oxidation, the calculation of the interdiffusion coefficient $\tilde{D}_{Ni\text{-}30Cr}$ is of great importance. For this purpose, the following equations given by Wagner [10] can be used.

$$\frac{N_{Cr}^{*} - N_{Cr}^{i}}{1 - N_{Cr}^{i}} = \mathbf{F}\left(\frac{k_c}{2\tilde{D}_{Ni-30Cr}}\right)^{1/2} \qquad \text{Equation 1}$$

N_{Cr}^{*} is the atomic fraction of chromium in the core of the alloy, while N_{Cr}^{i} is the atomic fraction of chromium at the alloy/scale interface and k_c is the parabolic rate constant for the alloy/scale interface recession in $cm^2\ s^{-1}$.

Moreover,

$$\mathbf{F}(u) = \pi^{1/2} u(1 - \operatorname{erf} u)\exp(u^2)$$ Equation 2

with

$$\mathbf{F}(u) \approx \pi^{1/2} u$$ Equation 3

when u << 1.

The validity of Eq. 1 is verified when the following conditions are fulfilled:

i) The system is in steady-state regime: the chromium contents in the core of the alloy and at the alloy/oxide interface must remain constant. As shown by Fig. 3 and Table 1, these requirements are valid for oxidation durations superior to 49 h in all tested atmospheres. This duration is consistent with the one deduced from oxidation kinetics in the first part of this work [20].

ii) A recession of the alloy/scale interface is considered. If all vacancies created at the interface by the incorporation of chromium into the scale are annihilated [19], this recession is directly linked to the growth rate of the oxide and the volume ratio of the oxide and the alloy by Eq. 4.

$$k_c = \left(2\frac{V_{Ni-30Cr}}{V_{Cr_2O_3}}\right)^2 k_{pe}$$ Equation 4

where $V_{\text{Ni-30Cr}}$ and $V_{Cr_2O_3}$ are the molar volumes of the alloy and the oxide respectively equal to 6.8 and 29.2 $cm^3\ mol^{-1}$. k_{pe} is the parabolic rate constant for oxidation of the alloy and is equal to 5.0 x 10^{-12} $cm^2\ s^{-1}$ [20]. The value obtained for k_c is therefore 1.1 x 10^{-12} $cm^2\ s^{-1}$.

iii) The interdiffusion coefficient is assumed to be independent on the alloy composition. This condition, even being little realistic, is mandatory for the use of analytical solutions derived from Fick's equation.

For calculations, N_{Cr}° is taken equal to 0.331 *i.e.* the atomic fraction of chromium in the as-prepared alloy and N_{Cr}^{i} equal to 0.242, the average atomic fraction of chromium at the alloy/scale interface for oxidation durations superior to 49 h (Table 1). Then, calculations with Eq. 1, 3 and 4 give a value for $\tilde{D}_{\text{Ni-30Cr}}$ equal to 1.2 x 10^{-10} $cm^2\ s^{-1}$ at 1150 °C.

This value is reported in an Arrhenius diagram on Fig. 6 with other values of interdiffusion coefficient in Ni-based alloys from other authors [14,17,18,27-29]. A good agreement is found between the present result and the data available in literature, considering the following Arrhenius fit for austenitic binary Ni-Cr alloys:

$$\tilde{D}_{Ni-Cr} = 0.1 \exp\left(\frac{-240000}{RT}\right) \qquad \text{Equation 5}$$

with the activation energy expressed in J mol^{-1} and the pre-exponential factor in cm^2 s^{-1}.

Based on the same assumptions as above, Eq. 6 describes the depletion profile of chromium in the case of a moving alloy/scale interface, where x is the position from the alloy/scale interface at time t [9,11].

$$N_{Cr}(x,t) = N_{Cr}^{i} + \left(N_{Cr}^{*} - N_{Cr}^{i}\right) \frac{\operatorname{erf}\left(\frac{x + \sqrt{2k_c t}}{2\sqrt{\tilde{D}_{Ni-Cr} t}}\right) - \operatorname{erf}\left(\sqrt{\frac{k_c}{2\tilde{D}_{Ni-Cr}}}\right)}{\operatorname{erfc}\left(\sqrt{\frac{k_c}{2\tilde{D}_{Ni-Cr}}}\right)} \qquad \text{Equation 6}$$

Fig. 7 shows the comparison between the fitted profiles, calculated with Eq. 6, and the experimental chromium profiles in the alloy, at steady-state, after different oxidation durations in 2.8 x 10^{-13} atm O_2. Fitted profiles are in good agreement with the experiment even though small deviations can be observed. These deviations may either be explained by the presence of vacancies affecting the activity of metallic elements [30] or most probably by the fact that the interdiffusion coefficient is dependent on the alloy composition. Wulf *et al.* [31] have used a numerical model in order to take into consideration the variation of the interdiffusion coefficient in a Fe-48Cr model alloy. By comparing their calculated profiles with others obtained by analytical or numerical methods without variation of the interdiffusion coefficient, differences in the shape of the profile are visible. Particularly near the alloy/scale interface, where the decrease of the chromium content is less sharp when the variation of the interdiffusion coefficient is considered. This is in accordance with the fact that the interdiffusion coefficient increases with decreasing chromium content in the composition range from 20 to 50 wt.% Cr in the Fe-Cr system [31]. Same features are visible in Fig. 7 as they can logically be expected in Ni-30Cr alloys since the interdiffusion coefficient also increases with decreasing chromium content in f.c.c. Ni-Cr lattice [14,32].

3. Lifetime estimation

The chemical lifetime of the alloy is related to its ability to develop continuous chromia scale. This consideration is particularly justified, for instance, in the case of corrosion by molten glasses. Indeed the protection of alloys against corrosion by molten glass is provided by a Cr_2O_3 layer since it has the lower solubility in molten glasses amongst refractory oxides [33-35]. The conditions for selective formation of external Cr_2O_3 are fulfilled when two criterions are satisfied. First, the chromium content at the alloy/scale interface must be high enough to allow the selective external oxidation of chromium. Second, the diffusion of chromium in the alloy must be rapid enough to compensate at least the amount of chromium that is incorporated in the oxide scale.

The first criterion given by Wagner [10,36] is, in the case of Ni-Cr alloys:

$$N_{Cr}^{i} \geq \left[\frac{\pi g^{*}}{2\nu} N_{O}^{(s)} \frac{D_{O}.V_{Ni-Cr}}{\tilde{D}_{Ni-Cr}.V_{CrO_{\nu}}}\right]^{1/2} \qquad \text{Equation 7}$$

g^* is the fraction of internal oxides in the alloy from which the transition from internal to external oxidation occurs. Its value is generally taken equal to 0.3 from [37]. $V_{CrO\nu}$ is the molar volume of CrO_ν (here ν = 1.5) and is equal to 14.6 cm^3 mol^{-1}. $N_O^{(s)}$ is the oxygen solubility in the alloy and is approximated from measurements in pure nickel [38] and taken equal to 800 ppm. D_O is the oxygen diffusion coefficient in the alloy, approximated to that in pure nickel, which is equal to 4.7 x 10^{-8} cm^2 s^{-1} [38]. The product of these two parameters is in good agreement with the values of oxygen permeability in Ni-Cr alloys, $N_O^{(s)}D_O$, determined by Guo *et al.* at 1100 °C [39].

According to Eq. 7, the minimum chromium content at the alloy/scale interface for the selective oxidation of chromium in Ni-30Cr at 1150 °C is about 21.4 at.% (= 19.4 wt.%). This value is compatible with the interfacial chromium content at steady-state obtained in this work (Fig. 3 and Table 1). For shorter oxidation duration (< 49 h), *i.e.* during transitory regime, the value for interdiffusion coefficient $\tilde{D}_{Ni\text{-}Cr}$ near the alloy/scale interface may be higher than the one used for calculation because of the composition variation in the depleted alloy [14,32]. Therefore according to Eq. 7, a higher interdiffusion coefficient would lead to a lower critical value for N_{Cr}^{i} as it is observed (Fig. 3 and Table 1). For example, for the minimum observed interfacial chromium content (12 wt.% (= 13.3 at.%)), the interdiffusion coefficient calculated

from Eq. 7 is equal to 3.1 x 10^{-10} cm^2 s^{-1}. This value is 2.5 times higher than the interdiffusion coefficient obtained in steady-state conditions.

Regarding the second criterion, for a system with fixed alloy/scale interface, Wagner [9] gave an expression for the minimum chromium content difference through the alloy to satisfy this second criterion. However, in the case of a moving alloy/scale interface, Wagner's equation in [9] has been developed by Bastow *et al.* and the second criterion is given by the following equation [11]:

$$N_{Cr} - N_{Cr}^{i} \geq \frac{V_{Ni-Cr}}{V_{Cr_2O_3}} \sqrt{\frac{\pi k_{pe}}{2\tilde{D}_{Ni-Cr}}} \left(1 - N_{Cr}^{i}\right). \operatorname{erfc}\left(\sqrt{\frac{k_c}{2\tilde{D}_{Ni-Cr}}}\right) \exp\left(\frac{k_c}{2\tilde{D}_{Ni-Cr}}\right) \quad \text{Equation 8}$$

Eq. 8 reduces to Wagner's expression in [9] when $N_{Cr}^{i} << 1$ and $k_c = 0$.

According to Eq. 8, the necessary chromium content difference to sustain the chromium consumption is about 4.3 at.%.

Thus, protection of the alloy (external Cr_2O_3 growth) is ensured as long as the chromium content is at least 21.4 at.% at the interface and 25.7 at.% in the core of the alloy. Therefore, the end of life of the alloy arise when the chromium depletion reaches 25.7 at.% in the core of the alloy.

Then, the chemical lifetime of the alloy t (in s), can be estimated with Eq. 6 (with $N_{Cr}^{i} = 0.214$ and $N_{Cr(x,t)} = 0.257$). In Eq. 6, x represents the position in the alloy with respect to the mobile alloy/oxide interface, whereas the product $\sqrt{(2k_c t)}$ represents the recession of this interface. Therefore the sum of these two terms represents the position in the alloy with respect to the initial alloy/gas interface(in cm). For the purpose of illustration, a 0.5 mm thick sample submitted to a continuous one-side oxidation at 1150 °C would have a lifetime of 1 year.

It is noteworthy that the use of Eq. 6 in order to estimate the chemical lifetime of alloys is applicable to various types of high temperature corrosion (atmospheric oxidation, corrosion by molten glasses or salts, etc…) as long as a protective oxide is covering the surface of the alloy. Indeed, Eq. 6 is based on the diffusion phenomena in the alloy. Therefore, since the diffusion through the oxide is much slower than in the alloy, depletion profiles would remain unaffected by the presence of corrosive phases as long as a protective oxide layer is present. In the case of corrosion by a surrounding phase, the integrity of the protective layer is

dependent, on the competition between its formation and its destruction by reaction or dissolution in the media [34,35].

The chemical lifetime would obviously be lowered when considering oxide spallation that can occur in the case of cyclic oxidation or oxidation under mechanical strain for instance. Indeed, every oxide fracture event will lead to a local acceleration of the oxidation kinetics [5,6]. In the case of cyclic oxidation, taking into account the spallation phenomenon, in order to modify the k_c parameter in Eq. 6, requires the knowledge of several parameters such as (i) the location and the extent of spallation sites (in the case of external oxide growth, spallation is favoured above the alloy grain boundaries and is enhanced in high oxygen pressure [20]), (ii) the frequency of oxidation cycles (since a sufficient time is required to reach steady-state regime [20]) and (iii) the cooling and heating rates (which affect thermal stresses in the scale).

4. Modelling of the oxidation of Ni-30Cr alloy

A summary of the phenomena encountered in Ni-30Cr system oxidised at 1150 °C in oxygen atmospheres in proposed here. Results from part I [20] and II (present paper) of this work are gathered in this section.

(i) In the oxide phase [20], only pure Cr_2O_3 is formed during steady-state regime by reaction between chromium from the alloy and oxygen from the atmosphere. The oxide grows by outward diffusion of chromium interstitials. Furthermore, the high value of the calculated self-diffusion coefficient of chromium in the oxide (5.0×10^{-12} cm^2 s^{-1}) gives evidence of rapid diffusion of chromium along grain boundaries.

With the aim of establishing a predictive model to calculate the lifetime of the alloy, the oxidation kinetics and mechanism must be known. For austenitic chromia-forming alloys, the oxidation kinetics is generally described with the parabolic rate constant. This latter can be obtained experimentally or estimated from appropriate data on the defects concentration and their diffusion coefficients.

(ii) In the metallic phase, a chromium depletion profile is created, consecutively to the incorporation of chromium from the alloy into the oxide. At steady-state regime, the chromium content at the alloy/scale interface stabilises when the chromium fluxes in the alloy and in the scale equilibrate. Regarding the depletion profile, it becomes deeper with increasing time. Besides, the fitting of depletion profiles with Eq. 6 provides a good matching

with the experimental results (Fig. 7). In addition, this profile leads to a counter-diffusion of chromium (towards the oxide) and nickel (towards the core of the alloy). As chromium diffuses faster, a vacancies flux is created in order to equilibrate the flux balance and pores formation can arise after their condensation.

A schematic representation of the oxidation processes of Ni-30Cr alloy at 1150 °C in intermediate oxygen atmospheres is then presented in Fig. 8. The ordinate qualitatively represents the chemical potential of chromium in the alloy and in the oxide layer; and the abscissa qualitatively represents the position in the alloy-oxide-atmosphere system. z_0 is the position of the alloy/scale interface, taken as the referential position (x = 0) in Eq. 6. z_{oxide} is the position of the oxide/atmosphere interface, which also corresponds to the oxide thickness with respect to the referential position z_0.

Eventually, the long-term behaviour of the alloy can be predicted with Eq. 6 to 8, provided that parameters N_{Cr}^{i}, $\tilde{D}_{Ni\text{-}Cr}$, k_{pe}, D_O, $N_O^{(s)}$ and g^* are known or can be approximated.

Conclusions

Chromium depletion in chromia-forming Ni-30Cr alloy has been apprehended in this paper. Samples have been oxidised at 1150 °C up to 289 h in oxygen partial pressures between 10^{-13} and 10^{-3} atm. After oxidation, the presence of Kirkendall pores and a chromium depleted zone under the oxide scale have been observed in the alloy matrix.

The analysis of depletion profiles led to the calculation of the interdiffusion coefficient of chromium in the alloy, $\tilde{D}_{Ni\text{-}30Cr}$, which is equal to 1.2 x 10^{-10} cm^2 s^{-1} at 1150 °C. Furthermore, analytical solutions for a stationary system with alloy/scale interface recession have been used to fit the depletion profiles with good accuracy. Eventually, a predictive chemical lifetime model for the oxidation of austenitic chromia-forming Ni-Cr alloys is provided, based on the criterion that the end of life of the alloy occurs when the chromium depletion in the alloy becomes overly significant (in terms of critical interfacial chromium content and critical chromium concentration gradient). In that case, the alloy is not able to form a protective pure Cr_2O_3 layer anymore. For this model, the oxidation mechanisms and kinetics, as well as the chromium interdiffusion coefficient and the chromium concentration at the alloy/scale interface must be known.

Acknowledgements

The authors are grateful to S. Mathieu and O. Rouer for their helpful contributions in SEM characterisations and EPMA analyses.

References

[1] H.E. Evans, A.T. Donaldson, T.C. Gilmour, Mechanisms of breakaway oxidation and application to a chromia-forming steel, Oxid. Met. 52 (1999) 379-402.

[2] W.J. Quadakkers, K. Bongartz, The prediction of breakaway oxidation for alumina forming ODS alloys using oxidation diagrams, Mater. Corros. 45 (1994) 232-241.

[3] M.M. Nagl, W.T. Evans, The mechanical failure of oxide scales under tensile or compressive load, J. Mater. Sci. 28 (1993) 6247-6260.

[4] M. Schütze, Mechanical properties of oxide scales, Oxid. Met. 44 (1995) 29-61.

[5] C.E. Lowell, C.A. Barrett, R.W. Palmer, J.V. Auping, H.B. Probst, COSP: A computer model of cyclic oxidation, Oxid. Met. 36 (1991) 81-112.

[6] D. Poquillon, D. Monceau, Application of a simple statistical spalling model for the analysis of high-temperature, cyclic-oxidation kinetics data, Oxid. Met. 59 (2003) 409-431.

[7] W.G. Kim, S.N. Yin, G.G. Lee, Y.W. Kim, S.J. Kim, Creep oxidation behaviour and creep strength prediction for Alloy 617, Int. J. Pres. Ves. Pip. 87 (2010) 289-295.

[8] P. Berthod, L. Aranda, Thermal expansion behaviour of ternary nickel-based, cobalt-based, and iron-based alloys containing very high fractions of carbides, ISRN Metall. 2012, (2012) 1-9.

[9] C. Wagner, Theoretical analysis of the diffusion processes determining the oxidation rate of alloys, J. Electrochem. Soc. 99 (1952) 369-380.

[10] C. Wagner, Reaktionstypen bei der Oxydation von Legierungen, Z. Electrochem. 63 (1959) 772-782.

[11] B.D. Bastow, D.P. Whittle, G.C. Wood, Alloy depletion profiles resulting from the preferential removal of the less noble metal during alloy oxidation, Oxid. Met. 12 (1978) 413-438.

[12] F. Gesmundo, Transient state in the selective oxidation of binary alloys with quasiparabolic kinetics: Solution for a fixed alloy-scale boundary, Oxid. Met. 12 (1978) 205-214.

[13] T. Hodgkiess, G.C. Wood, D.P. Whittle, B.D. Bastow, Compositional changes in the underlying alloy produced by the oxidation of Ni-Cr alloys, Oxid. Met. 12 (1978) 439-449.

[14] D.P. Whittle, D.J. Evans, D.B. Scully, G.C. Wood, Compositional changes in the underlying alloy during the protective oxidation of alloys, Acta Metall. 15 (1967) 1421-1430.

[15] T.J. Nijdam, L.P.H. Jeurgens, W.G. Sloof, Modelling the thermal oxidation of ternary alloys—compositional changes in the alloy and the development of oxide phases, Acta Mater. 51 (2003) 5295-5307.

[16] T.J. Nijdam, W.G. Sloof, Modelling of composition and phase changes in multiphase alloys due to growth of an oxide layer, Acta Mater., 56 (2008) 4972-4983.

[17] R. Pillai, H. Ackermann, K. Lucka, Predicting the depletion of chromium in two high temperature Ni alloys, Corros. Sci. 69 (2013) 181-190.

[18] A. Chyrkin, W.G. Sloof, R. Pillai, T. Galiullin, D. Grüner, L. Singheiser, W.J. Quadakkers, Modelling compositional changes in nickel base alloy 602 CA during high temperature oxidation, Mater. High Temp. 32 (2015) 102-112.

[19] C. Desgranges, F. Lequien, E. Aublant, M. Nastar, D. Monceau, Depletion and voids formation in the substrate during high temperature oxidation of Ni–Cr alloys, Oxid. Met. 79 (2013) 93-105.

[20] E. Schmucker, C. Petitjean, L. Martinelli, P.J. Panteix, S. Ben Lagha, M. Vilasi, Oxidation of Ni-Cr alloy at intermediate oxygen pressures. I. Diffusion mechanisms through the oxide layer, Submitted to Corros. Sci. (2016)

[21] W. Huang, Y.A. Chang, Thermodynamic properties of the Ni–Al–Cr system, Intermetallics, 7 (1999) 863-874.

[22] A.H. Rosenstein, J.K. Tien, W.D. Nix, Void formation in INCONEL MA-754 by high temperature oxidation, Metall. Trans. A 17 (1986) 151-162.

[23] Y. Shida, G.C. Wood, F.H. Stott, D.P. Whittle, B.D. Bastow, Intergranular oxidation and internal void formation in Ni-40% Cr alloys, Corros. Sci. 21 (1981) 581-597.

[24] E.O. Kirkendall, Diffusion of zinc in alpha brass, Trans. Met. Soc. AIME 147 (1942) 104-109.

[25] J. Růžičková, B. Million, Self-diffusion of the components in the F.C.C. phase of binary solid solutions of the Fe-Ni-Cr system, Mater. Sci. Eng. 50 (1981) 59-64.

[26] K. Monma, H. Suto, H. Oikawa, Diffusion of ^{63}Ni and ^{51}Cr in nickel chromium alloys, J. Jpn. I. Met. 28 (1964) 188-192.

[27] B. Li, B. Gleeson, Effects of silicon on the oxidation behavior of Ni-base chromia-forming alloys, Oxid. Met. 65 (2006) 101-122.

[28] N. Garimella, Y. Sohn, M.P. Brady, Interdiffusion in γ (face-centered cubic) Ni-Cr-X (X= Al, Si, Ge, or Pd) alloys at 900° C, J. Phase Equilib. Diff. 27 (2006) 665-670.

[29] T. Hodgkiess, G.C. Wood, D.P. Whittle, B.D. Bastow, The oxidation of Ni-70 wt.% Cr in oxygen between 1073 and 1473° K, Oxid. Met. 14 (1980) 263-277.

[30] G.B. Gibbs, R. Hales, The influence of metal lattice vacancies on the oxidation of high temperature materials, Corros. Sci. 17 (1977) 487-507.

[31] G.L. Wulf, M.B. McGirr, G.R. Wallwork, Theoretical analysis of alloy oxidation with reference to Fe-Cr alloys, Corros. Sci. 9 (1969) 739-754.

[32] B. Million, J. Růžičková, J. Vřešťál, Diffusion in Fe-Ni-Cr alloys with an FCC lattice, Mater. Sci. Eng. 72 (1985) 85-100.

[33] L.J. Manfredo, R.N. McNally, Solubility of Refractory Oxides in Soda-Lime Glass, J. Am. Ceram. Soc. 67 (1984) C155-C158.

[34] C. Petitjean, P.J. Panteix, C. Rapin, M. Vilasi, R. Podor, Electrochemical Behavior of Glass Melts: Application to Corrosion Processes, Procedia Materials Science 7 (2014) 101-110.

[35] T. Gheno, G.H. Meier, B. Gleeson, High Temperature Reaction of MCrAlY Coating Compositions with CaO Deposits, Oxid. Met. 84 (2015) 185-209.

[36] E. Essuman, G.H. Meier, J. Zurek, M. Hänsel, T. Norby, L. Singheiser, W.J. Quadakkers, Protective and non-protective scale formation of NiCr alloys in water vapour containing high- and low-pO_2 gases, Corros. Sci. 50 (2008) 1753-1760.

[37] R.A. Rapp, The transition from internal to external oxidation and the formation of interruption bands in silver-indium alloys, Acta Metall. 9 (1961) 730-741.

[38] J.W. Park, C.J. Altstetter, The diffusion and solubility of oxygen in solid nickel. Metall. Trans., A 18 (1987) 43-50.

[39] P. Guo, J. Zhang, D.J. Young, C.H. Konrad, Oxygen permeability measurements in Ni using H_2/H_2O, CO/CO_2 and Ni/NiO Rhines pack atmospheres, Oxid. Met. 83 (2015) 223-235.

Tables

Table 1: Interfacial chromium content W_{Cr}^{i} (determined from profiles fit with Eq. 6), chromium depletion depth X_{Cr} (read on experimental profiles) and pores formation depth X_{pores} in the alloy for every tested times and atmospheres at 1150 °C.

$P(O_2)$ (atm)		1h	4h	9h	16h	25h	49h	100h	289h
	W_{Cr}^{i} (wt.%)	15	16	18	19	21	21	22	22.5
2.8×10^{-13}	X_{Cr} (µm)	≥ 70	80	100	> 110	≥ 140	> 170	300	500
	X_{pores} (µm)	40	50	90	100	120	120	-	-
	W_{Cr}^{i} (wt.%)	17*	17	18	19	19.5	20	22	21
5.8×10^{-12}	X_{Cr} (µm)	> 50*	> 70	> 100	> 130	> 140	> 160	300	460
	X_{pores} (µm)	30*	80	110	120	130	140	180	250
	W_{Cr}^{i} (wt.%)	12	14	-	19	19	20	-	-
4.2×10^{-10}	X_{Cr} (µm)	70	70	-	> 130	≥ 160	≥ 200	-	-
	X_{pores} (µm)	-	60	-	110	-	130	-	-
	W_{Cr}^{i} (wt.%)	12	16	18	19	21	22	22	23
5.9×10^{-3}	X_{Cr} (µm)	80	100	120	130	≥ 180	≥ 200	300	500
	X_{pores} (µm)	-	70	-	-	160	170	180	250

*1h30

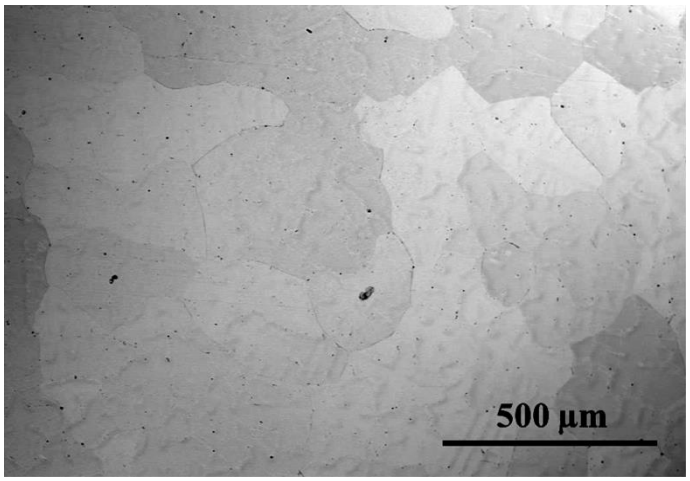

Figure 1: BSE image of the microstructure of the as-prepared Ni-30Cr alloy after chemical etching in *aqua regia*.

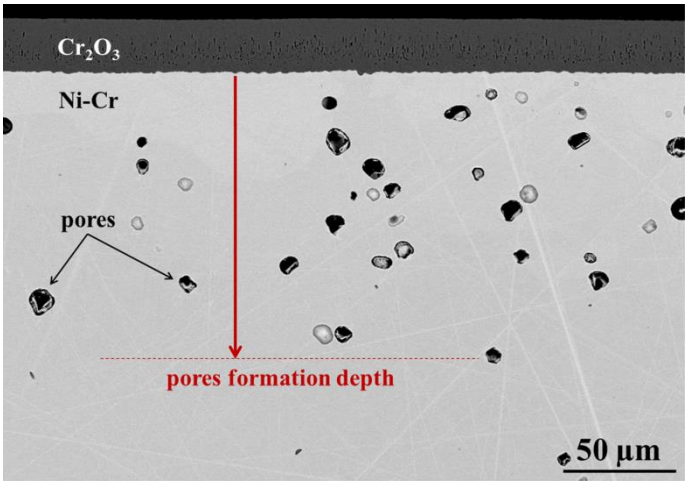

Figure 2: BSE cross-section image of Ni-30Cr oxidised for 49 h in 2.8 x 10^{-13} atm O_2 at 1150 °C showing the formation of pores in the alloy.

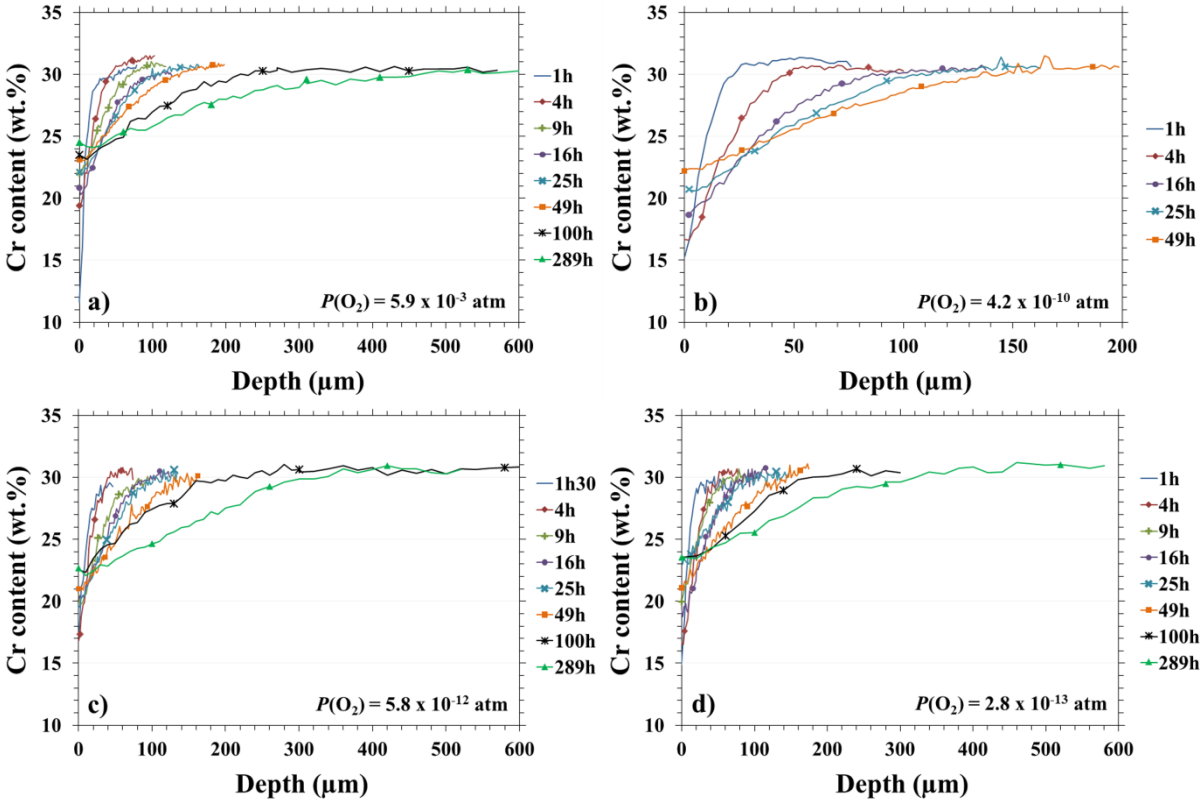

Figure 3: Chromium depletion profiles in Ni-30Cr alloy after oxidations at 1150 °C a) in 5.9 x 10^{-3} atm O_2; b) in 4.2 x 10^{-10} atm O_2; c) 5.8 x 10^{-12} atm O_2; d) 2.8 x 10^{-13} atm O_2.

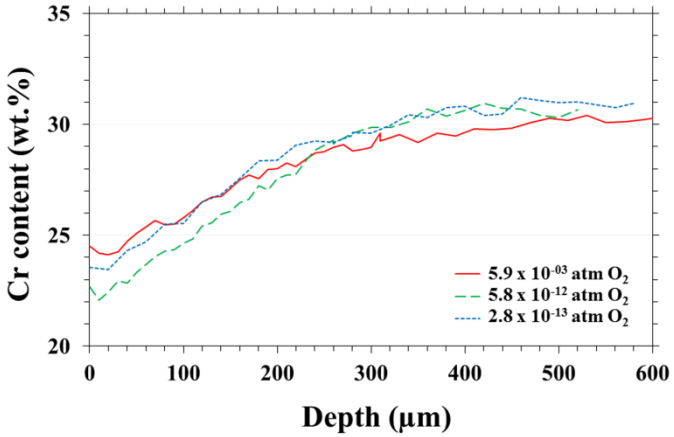

Figure 4: Chromium depletion profiles in Ni-30Cr after oxidations of 100h in different oxygen partial pressures at 1150 °C.

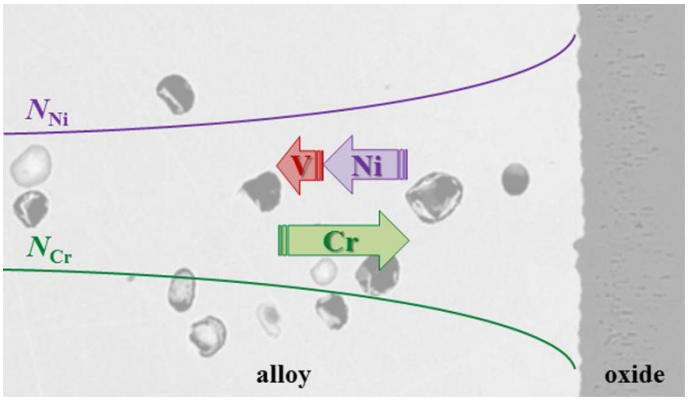

Figure 5: Schematic representation of Kirkendall fluxes in NiCr alloy.

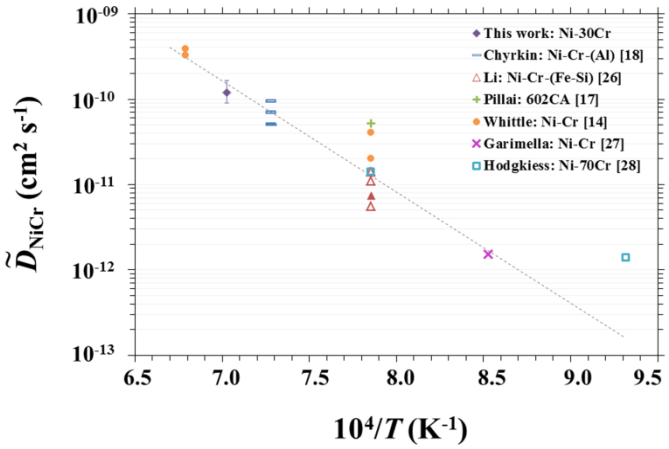

Figure 6: Arrhenius plot of interdiffusion coefficients in nickel-based alloys. Filled symbols represent data for pure austenitic binary Ni-Cr alloys. Dashed line is a fit of data from pure binary austenitic alloys (with pre-exponential factor equal to 0.1 cm^2 s^{-1} and activation energy equal to 240 kJ mol^{-1}).

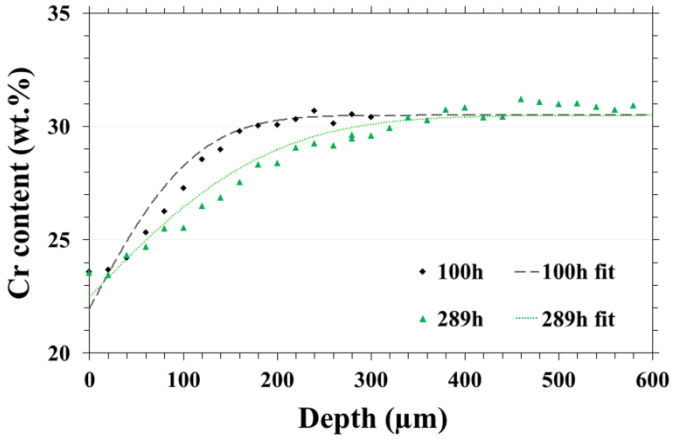

Figure 7: Comparison between experimentally determined chromium depletion profiles (in Ni-30Cr alloy oxidised in 2.8 x 10^{-13} atm O_2 at 1150 °C) and analytical fits obtained with Eq. 6.

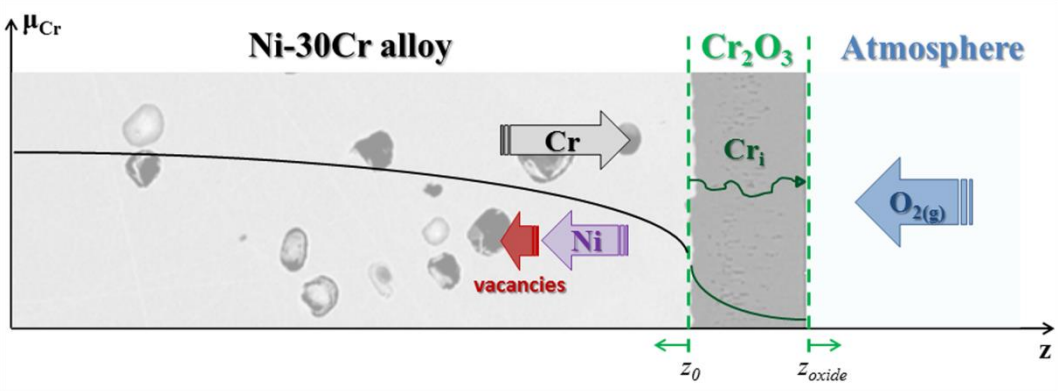

Figure 8: Schematic representation of the oxidation processes of Ni-30Cr alloy at 1150 °C in intermediate oxygen atmospheres.